**International Journal of Physical Modelling in Geotechnics**
Volume 18 Issue 2

**The effect of spherical air blast on buried pipelines: a laboratory simulation study**
Vivek and Sitharam

International Journal of Physical Modelling in Geotechnics, 2018, **18**(2), 57–67
https://doi.org/10.1680/jphmg.16.00070
**Paper 1600070**
Received 04/11/2016 Accepted 06/06/2017
Published online 30/06/2017
**Keywords:** dynamics/granular materials/pipes & pipelines



ice Institution of Civil Engineers
publishing

# The effect of spherical air blast on buried pipelines: a laboratory simulation study

**Padmanabha Vivek** PhD
Research Scholar, Department of Civil Engineering, Indian Institute of Science, Bangalore, India (corresponding author: vivek2387@gmail.com) (Orcid:0000-0002-0047-5642)

**Thallak G. Sitharam** PhD
Professor, Department of Civil Engineering, Indian Institute of Science, Bangalore, India

**A new laboratory-scale experimental technique has been developed to study the blast wave effects on buried pipelines caused by an explosion at an altitude. A shock tube is used in this study to generate a blast wave in a controlled and repeatable manner, without the use of any explosives. The blast wave profile generated is characterised by peak reflected pressure and positive phase duration and is represented using tri-nitro-toluene equivalents. Shock tube experiments have been carried out on a reduced-scale pipe model in a sand deposit. The momentum transfer from the blast wave to the sand bed is indicated by the presence of compression stress waves. It is demonstrated from the experiments that the shock tube is an effective and versatile tool for investigating the interactions of blast wave with the buried structures. Using the dimensional analysis procedure, shock tube experimental results are scaled up to predict the real-scale damage imparted to the buried pipes during a spherical air-burst explosion. In addition, a three-dimensional finite-element analysis of the test condition is performed to investigate the fidelity of the scaling laws.**

## Notation

| | |
|---|---|
| $b$ | decay coefficient |
| $D_{50}$ | sieve size with 50% by mass passing |
| $E$ | elastic modulus of the pipe |
| $E_s$ | elastic modulus of sand |
| $e_{max}$ | maximum void ratio of sand |
| $e_{min}$ | minimum void ratio of sand |
| $H$ | depth of the test chamber |
| $I$ | moment of inertia of the pipe |
| $I_b$ | positive impulse |
| ID | inner diameter of the pipe |
| $L$ | width (length) of the test chamber |
| OD | outer diameter of the pipe |
| $P_a$ | ambient atmospheric air pressure |
| $P_4$ | rupture pressure of the diaphragm |
| $P_5$ | peak reflected side-on overpressure |
| $R$ | altitude of the explosion above the ground surface |
| $T$ | thickness of the pipe |
| $t_d$ | positive phase duration |
| $W$ | weight of the equivalent tri-nitro-toluene |
| $Z$ | scaled distance |
| $\delta$ | residual deflection of the pipe |
| $\varepsilon$ | strain experienced by the pipe |
| $\lambda$ | scaling coefficient |
| $\rho_s$ | dry density of sand |
| $\phi$ | friction angle of sand |

## 1. Introduction

The study of buried structures under impulsive loads induced by explosions has always been an important and challenging problem. In this study, buried oil pipelines are considered as potential targets; a possible attack on oil pipelines will lead to secondary explosion risking lots of lives and bring about immediate transit interruptions. Most of the explosives are set to detonate at an altitude above the ground, thereby inflicting maximum damage to the ground structures and it becomes very difficult to predict ground response and the damage inflicted on the underground structures. As the blast wave strikes the ground surface, shock waves travel through the ground causing damage to the underground pipelines. The extent of damage on the pipe would not only depend on the intensity of the blast wave but also on the properties of the embedded sand, depth of burial (Dob), and on the stiffness and geometry of the pipe structure. A considerable number of numerical simulations have been reported in the literature on the blast response of underground structures subjected to surface explosion (Koneshwaran *et al.*, 2015; Olarewaju *et al.*, 2010; Xu *et al.*, 2013; Zhang *et al.*, 2016). However, very few researchers have attempted to perform experiments on a real physical model. De and Zimmie (2007) have performed a series of surface explosion experiments on a reduced-scale (1:70 scales) model using a geotechnical centrifuge (De *et al.*, 2016). These centrifuge experiments provide quantitative information on buried structures exposed to a surface blast. Due to the high costs associated with full-scale field tests, risks involved using explosives and due to the difficulty in diagnostic measurements, there is a need for an alternative testing method. The shock tube-based tests can be considered as an effective alternative to the conventional testing methods (Aune *et al.*, 2016; Colombo *et al.*, 2011, 2013).

This paper proposes a new reduced-scale experimental technique for the testing of buried pipelines using a shock tube. A shock tube has been proven to be a simple and efficient tool for generating a blast wave (Aune *et al*., 2016; Kleinschmit, 2011; Newman and Mollendorf, 2010; Vivek and Sitharam, 2017). This study explores the performance of a compressed, gas-driven shock tube facility in generating a blast wave similar to free-field explosive detonations. The objective of this study is to develop an integrated testing facility to study blast wave interaction with the ground surface and the structures buried beneath it. Understanding the attenuation behaviour of sand plays a vital role in assessing the response of the buried pipe. This is done by comparing the pressure–time histories recorded at different depths of the sand deposit. Besides, the response of the pipe is monitored using dynamic strain measurements. Large full-scale prototype results are deduced from the results of the reduced-scale experiments using dimensional analysis. Finally, numerical simulation is performed to validate the predicated results obtained through scaling laws.

## 2. Experimental set-up

Let us consider an explosion in air at a few metres above the ground surface; a free-field air blast spherically expands striking the ground surface. The typical waveform of a free-field explosion is characterised by a shock front followed by non-linear decay (Chandra *et al*., 2012). The Friedlander wave equation is generally used to represent the pressure–time history of an ideal blast wave and it is given by the equation

$$P(t) = P_5\left(1 - \frac{t}{t_d}\right)e^{-bt/t_d} \quad (1)$$

### 2.1 Vertical shock tube

In this study, a vertical shock tube of 5 m long is used and it is divided into two main sections: driver and driven section, both sections have a constant internal diameter of 135 mm. The modular shock tube system enables us to configure shock tubes of varying lengths (driver and driven section). The driver section can be varied from 0·5 to 1·5 m long and the total length of the driven section is 4·5 m, with flexibility of varying lengths in increments of 0·5 m. The driver section contains the high-pressure gas, whereas the driven section is maintained at a low gas pressure (generally air at atmospheric pressure, $P_a$). These sections are separated by a metal diaphragm. Rubber O-rings are provided in the flange of the diaphragm mounting section to ensure sealing. The metal diaphragm is generally provided with a groove of specific depth, which ensures controlled rupture with repeatable bursting pressure. The diaphragm is ruptured using high-pressure driver gas. Following spontaneous rupture of the diaphragm, a series of compression waves are formed in the driven section, which eventually coalesce to form a shock front. Simultaneously, an expansion wave travel into the driver section and upon reflection from the driver end, the reflected expansion wave catches up with the shock front and decays the pressure levels.

In this work, the focus is to generate a near-ideal Friedlander wave at the exit of the shock tube. The shock tube is operated with the following test conditions: (*a*) driver section of 0·5 m with helium or nitrogen as driver gas, (*b*) a driven section of 4·5 m is maintained at standard room temperature and air at atmospheric pressure ($P_a$) and (*c*) a 2 mm thick aluminium diaphragm with a 0·8 mm groove. A digital pressure gauge is fixed at the driver tube to record the diaphragm rupture pressure ($P_4$) and piezoelectric pressure transducers are mounted at the end of the driven section to measure the pressure signals and Mach number. Mach number is defined as the ratio of velocity of the shock in a given medium to the velocity of the sound in the same medium. The maximum working pressure of the driver section is about 10 MPa, while the driven section and dump tank are limited to 5 and 1 MPa, respectively. The schematic diagram of the vertical shock tube system along with the photograph of the test set-up is shown in Figure 1.

### 2.2 Test chamber and sample preparation

The shock tube blast experiments are performed on a reduced-scale model and the tail end of the shock tube is connected to a 200 mm square test chamber. Dried river sand is used for the bed preparation; sand is classified as poorly graded with symbol 'SP' as per the Unified Soil Classification System. The $D_{50}$ of the sand is found to be 0·7 mm with $e_{min}$ and $e_{max}$ of 0·53 and 0·9, respectively. While preparing the sand bed, it is important to maintain a constant relative density, such that the same test conditions can be reproduced. For this purpose, the sand pluviation technique is used, where sand grain particles are rained down by maintaining a constant height of fall. In this study, the sand bed is prepared with a relative density of 63% with an approximate density of 1600 kg/m$^3$. An aluminium pipe with a diameter of 25 mm ($ID_{al}$) and a wall thickness ($T_{al}$) of 1·25 mm is clamped to the inside wall of the test chamber. The distance between the crown of pipe and the top surface of the sand bed is noted as Dob. The schematic diagram of the test chamber is shown in Figure 2(a). The geometrical and engineering properties of the pipe and sand deposit are listed under the input variables column in Table 1.

### 2.3 Instrumentation

The shock speed and pressure profiles are determined from the two (S1 and S2) piezo-electric-type pressure transducers

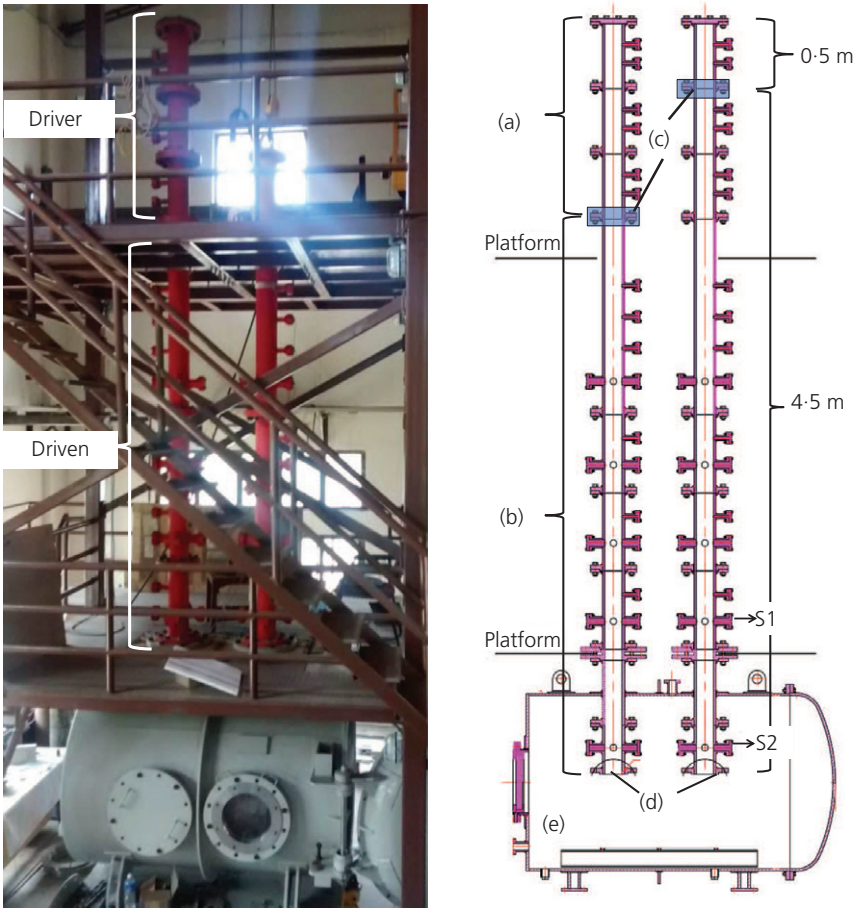


**Figure 1.** Left: photograph of the vertical shock tube; right: schematic diagram of the shock tube: (a) variable height driver section, (b) variable height driven section, (c) diaphragm mounting section, (d) tail end of the shock tube, (e) dump tank or collection chamber

(printed circuit board (PCB) 113A22) placed close to the tail end of the shock tube. Pressure/principal stresses in the sand deposit are measured using three (PT1, PT2 and PT3) embedded pressure transducers (PCB 113B22) placed at different depths of the test chamber (Figure 2). The pressure signals captured by PT1 will give the approximate pressure distribution around the pipe surface. The PCB transducers are in turn connected to a PCB signal conditioner (model 482A21). Two strain gauges (M/s IPA Pvt Ltd, India) are axially mounted on the top surface (crown) of the pipe; the axial strain response of the pipe is captured at two critical locations: crown, centre of the pipe (SG1) and at one-third span of the pipe (SG2). The strain gauge is connected in a quarter bridge Wheatstone configuration using DAQP-STG module of M/s Dewetron GmbH. Both pressure transducers and strain gauges data are acquired with a sampling rate of 1000 kHz using an oscilloscope (Yokogowa DL750).

## 3. Results and discussion

### 3.1 Evolution of a blast wave

Figure 3(a) shows the typical pressure–time history recorded at S2, a side-on pressure transducer just above the sand surface. With a shock tube pressure ratio (ratio of driver pressure, $P_4$ to the pressure in the driven section, $P_a$) of 13 and a rupture pressure of 1·3 MPa ($P_4$), two different pressure profiles are generated with nitrogen and helium as driver gas. With the former as driver gas, the pressure trace is characterised by the presence of incident shock front followed by a flat region and gradually increasing reflected overpressure. This waveform failed to incorporate the exponential decay immediately after the peak pressure as described in the previous section. However, using a lighter driver gas such as helium, a blast profile with an incident Mach number of 2·98 is generated, which closely matches with that of an ideal

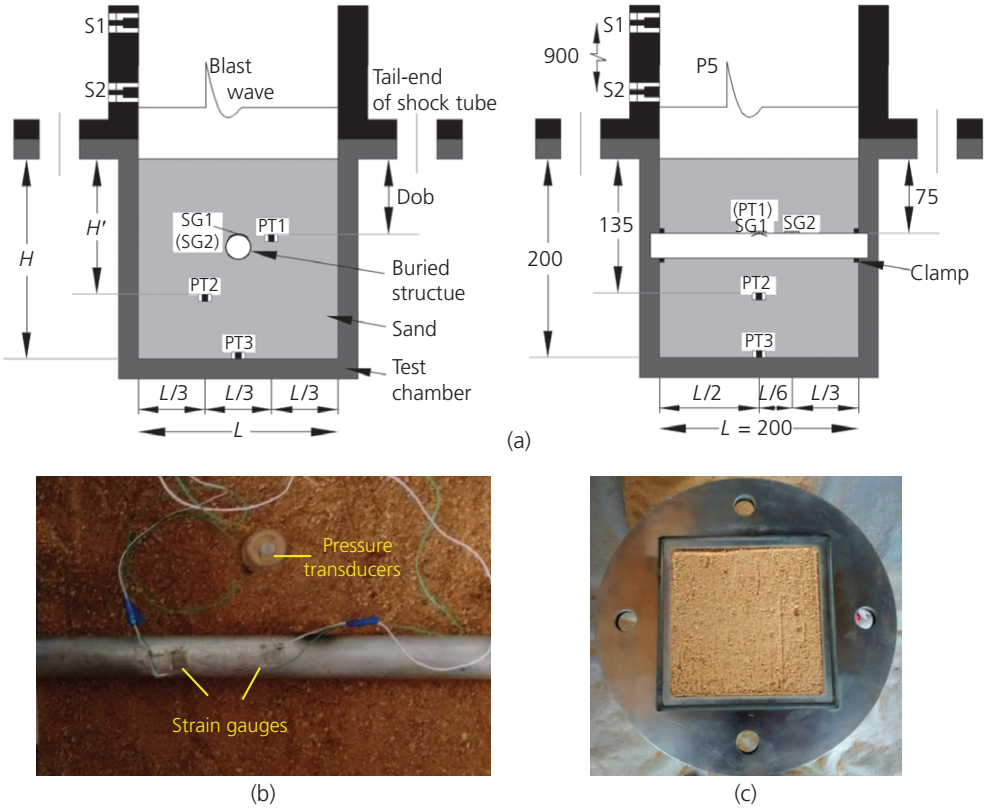


**Figure 2.** (a) Schematic diagram of the cross-sectional view of the test chamber showing the position of the buried pipe and the sensors (all dimensions are in mm), (b) photograph of the top view of the buried pipe, (c) photograph of the finished top surface of the sand deposit

**Table 1.** Input and output variables considered in this study

| Parameter | Dimension (MLT) | Experimental case 1 | Scaling factor | Predicted case 2 ($\lambda = 2$) |
|---|---|---|---|---|
| Input variables | | | | |
| Depth of burial, Dob | $M^0L^1T^0$ | 75 mm | $\lambda$ | 150 mm |
| Stiffness of pipe, EI | $M^1L^3T^{-2}$ | 613·6 N m$^2$ | $\lambda^4$ | 9818·3 N m$^2$ |
| Elastic modulus of sand, $E_s$ | $M^1L^{-1}T^{-2}$ | 15 MPa | 1 | 15 MPa |
| Dry density of sand, $\rho_s$ | $M^1L^{-3}T^0$ | 1606 kg/m$^3$ | 1 | 1606 kg/m$^3$ |
| Friction angle of sand, $\phi$ | — | 35° | 1 | 35° |
| Weight of equivalent tri-nitro-toluene (TNT), $W$ | $M^1L^0T^0$ | 20 kg | $\lambda^3$ | 160 kg |
| Altitude of explosion, $R$ | $M^0L^1T^0$ | 5 m | $\lambda$ | 10 m |
| Output variables | | | | |
| Positive phase duration, $t_d$ | $M^0L^0T^1$ | 3·34 ms | $\lambda$ | 6·68 ms |
| Peak reflected over pressure, $P_5$ | $M^1L^{-1}T^{-2}$ | 0·8 MPa | 1 | 0·8 MPa |
| Residual deflection of pipe at the crown (at $L/2$), $\delta$ | $L^1M^0T^0$ | 1·15 mm | $\lambda$ | 2·3 mm |
| Peak strain at crown (at $L/3$), $\varepsilon$ | $M^0L^0T^0$ | 700 μmm/mm | 1 | 700 μmm/mm |

Friedlander blast wave (Figure 3(a)). Two shock fronts (incident and reflected) are also identified; this is because the transducer (S2) which is located at an offset distance from the sand surface is bound to capture both incident and reflected shock wave passing against it. In all experiments conducted by the authors, it is assumed that the sand surface experienced

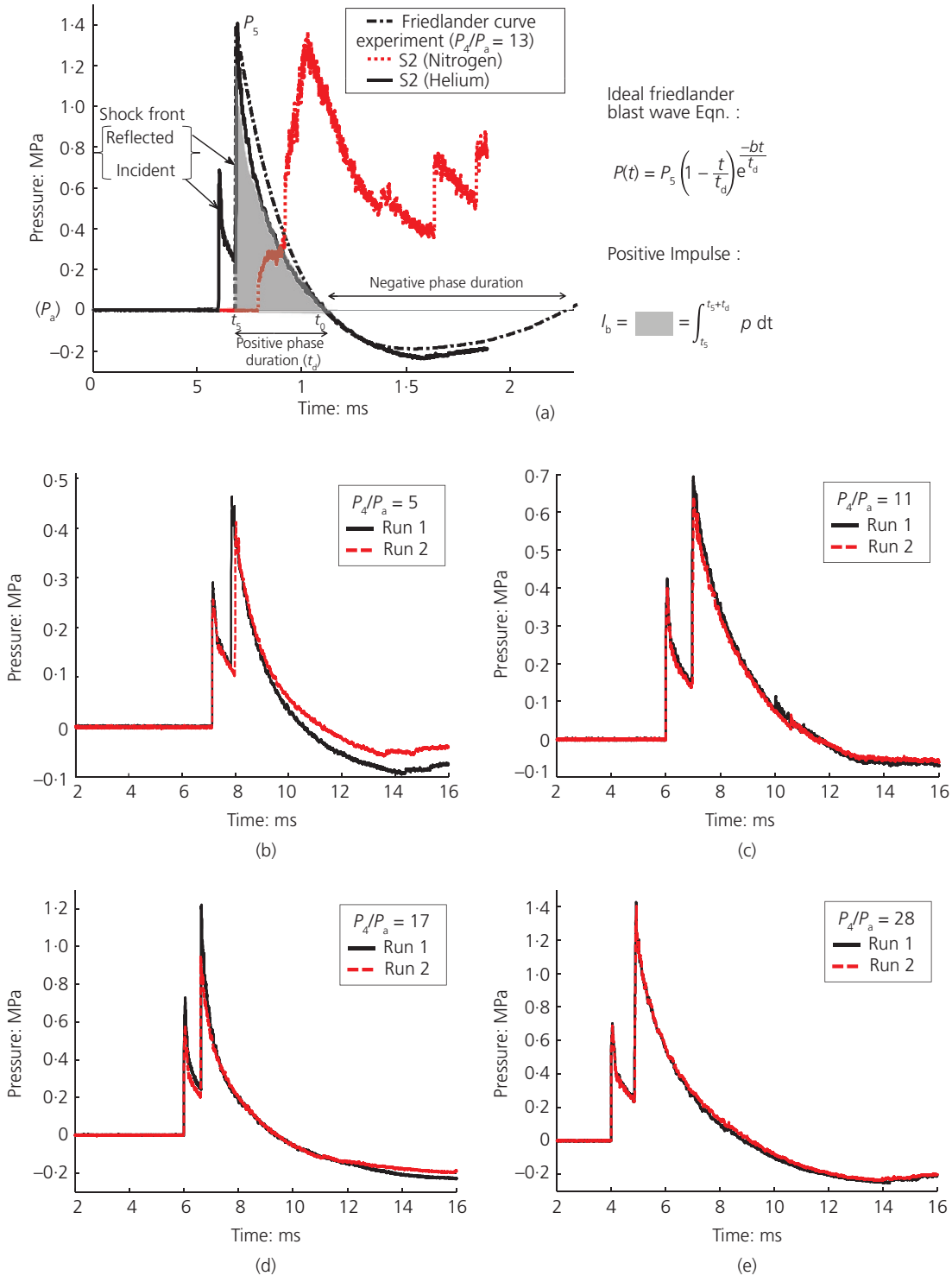


**Figure 3.** Pressure–time history recorded at transducer location, S2: (a) comparison of pressure profile recorded for nitrogen and helium with pressure ratio, $P_4/P_a = 13$; repeatable blast wave profile recorded for helium with pressure ratio, (b) $P_4/P_a = 5$, (c) $P_4/P_a = 11$, (d) $P_4/P_a = 17$, (e) $P_4/P_a = 28$

the same reflected overpressures recorded by S2. The duration of positive phase is the time taken for the peak reflected pressure ($t_5$) to decay to the atmospheric pressure levels ($t_0$) and the impulse is determined mathematically by calculating the area under the pressure–time curve over the positive phase duration ($t_d$). The peak reflected overpressure ($P_5$) and positive phase duration ($t_d$) are the blast parameters reported from the experiment and for a pressure ratio of 13, the blast parameters are found to be $P_5 = 0{\cdot}8$ MPa and $t_d = 3{\cdot}34$ ms.

Similar blast wave pressure profiles with different peak pressures and impulse are obtained by varying the shock tube pressure ratio. The pressure signals recorded by sensors have shown excellent signal repeatability. Figures 3(b)–3(e) show blast wave pressure signals recorded for two test runs of different pressure ratios ($P_4/P_a = 5$, 11, 17 and 28).

A summary of the pressure and impulse generated from the shock tube facility for the present test condition is shown in Figure 4; the graphical chart helps us to predict peak overpressure and impulse for a particular ratio of shock tube driver pressure to atmospheric pressure (driven). Furthermore, the blast parameters generated from the shock tube experiment can be related to an equivalent spherical air burst of tri-nitro-toluene (TNT) explosion (of weight '$W$') happening at an altitude of '$R$' above the ground surface. The most common scaling law for a blast wave is the cube-root scaling law (discussed later in Section 4), which uses scaled distance '$Z$' as a dimensional parameter. The '$Z$' parameter efficiently represents blast wave parameters for a wide range of detonation situation

$$2.\quad Z = \frac{R}{W^{1/3}}$$

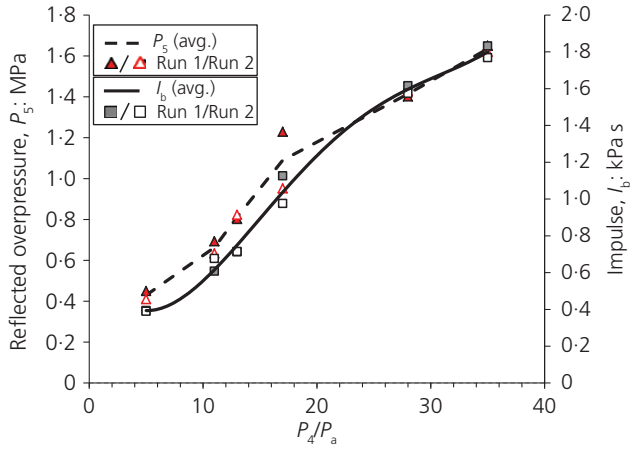


Figure 4. Plot of peak reflected pressure and impulse values against the ratio of shock tube pressure

The scaled distance value, $Z$, is calculated by applying the higher order polynomial coefficient (derived by Shin *et al.*, 2014) over the empirical relations (UFC 3-340-02 (USDoD, 2008)), representing the experimental data of Kingery and Bulmash (1984). The blast wave generated by the shock tube is indirectly compared with the TNT explosion using the Kingery and Bulmash (1984) charts. Table 2 compares the shock tube blast wave parameters with a practical TNT explosion of different weights detonating at different altitudes. The pressure–time history of signal S2 (helium) shown in Figure 3(a) corresponds to the pressure measurements made at the ground surface, when a 20 kg TNT explosive detonates at an altitude of 5 m. The buried pipe shock tube experiment is performed for this blast condition. It is important to note that the blast wave expanding radially from the source is assumed to have a planar shock front just before striking the ground surface. The blast wave generated can be tailored for a wide range of equivalent TNT by modifying the dimension of the driver (and driven) section of the shock tube, in addition to the rupture pressure ($P_4$).

### 3.2 Response of sand and buried pipes

When the shock front strikes the sand surface two important phenomena occur: first, an effective stress transfer takes place

Table 2. Shock tube blast parameters corresponding to an equivalent TNT explosion at distance $R$

| Shock tube blast parameters | | | Equivalent TNT spherical charge | | |
|---|---|---|---|---|---|
| Reflected side-on peak over pressure, $P_5$: MPa | Positive phase period, $t_d$: ms | Positive impulse, $I_b$: kPa s | Scaled distance, $Z$: m/kg$^{1/3}$ | Weight of TNT, $W$: kg | Altitude distance, $R$: m |
| 0·451 | 2·729 | 0·391 | 2·285 | 6·479 | 4·26 |
| 0·693 | 3·065 | 0·607 | 1·968 | 14·238 | 4·77 |
| 0·802 | 3·340 | 0·712 | 1·874 | 19·437 | 5·04 |
| 0·952 | 3·665 | 0·975 | 1·772 | 40·959 | 6·11 |
| 1·414 | 4·244 | 1·615 | 1·563 | 120·415 | 7·72 |
| 1·651 | 4·564 | 1·832 | 1·491 | 149·252 | 7·91 |

through particle–particle contact and second, the residual gas behind the shock front infiltrates through the sand deposit (Britan *et al.*, 1997). These mechanisms have degenerated the air-blast wave into compression wave in the sand. The compression stress signals measured by the transducers (PT1, PT2 and PT3) are shown in Figure 5 for the shock tube test case of $P_4/P_a$ equal to 13. The compression stress wave is characterised by a presence of sharp jump with a steady rise to a peak value followed by a gradual decrease in amplitude. The travelling compression wave is found to be planar and quickly attenuate with depth; pressure attenuation caused is about 60% of peak pressure value measured by the preceding transducer. The quantitative measurement inside the sand deposit may serve as an indicator of pressure imparted to the buried pipeline systems at different depths of the test chamber.

The blast effect on the pipe is characterised by observing the strain signals and the physical deformation of the pipe. As can be seen from Figure 6, a peak axial strain of 700 με is induced at one-third of the span. Due to the impact of the high-pressure compression wave, the strain gauge mounted at the centre of the span suffered damage and failed to capture the strain signal on both the test occasions. However, on excavating the pipe, the physical deflection of the pipe is evident at the centre of the crown surface (SG1). It is observed that the section along the pipe crown is compressed in the axial direction, while the invert section of the pipe is under tension (Koneshwaran *et al.* (2015) noticed a similar behaviour numerically). The maximum transverse deflection ($\delta_{max}$) at the crown of the pipe is expected to rebound after the passage of the compression waves, which is followed by a permanent

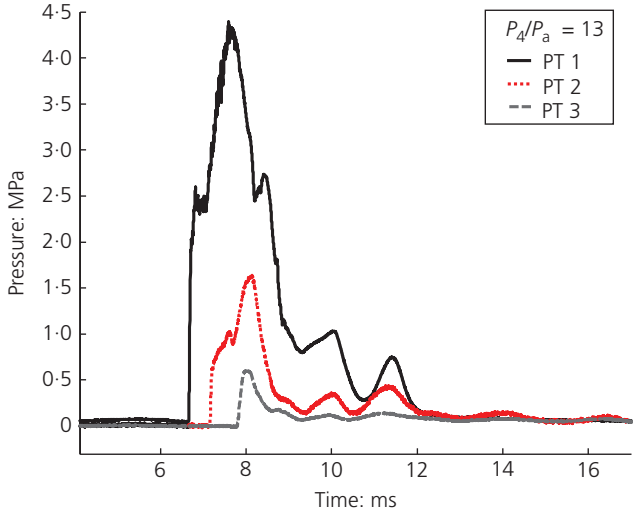


**Figure 5.** Compression stress signal measured inside the sand test chamber

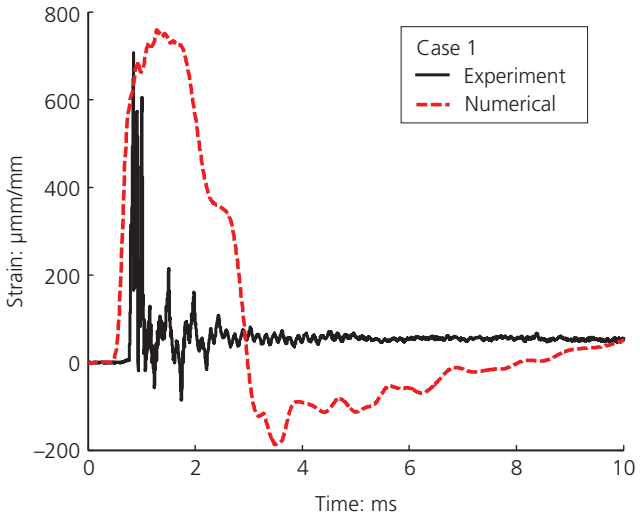


**Figure 6.** Strain histories measured at location of one-third span of the pipe for case 1

residual deflection (plastic deflection, $\delta$). The residual deflection of the pipe (at $L/2$ of the crown) is measured using a height gauge at the end of the experiment and is found to be 1·2 and 1·1 mm for run 1 and run 2, respectively; an average deflection value is considered for the dimensional analysis.

## 4. Dimensional analysis

Experiments performed using shock tube are however smaller than those of the actual site conditions. To bridge this scale issue, dimensional analysis is carried out using Buckingham $\pi$-theorems (Zhao *et al.*, 2013). Table 1 lists the input and output variables involved in the current experiment; the variables are expressed in the fundamental dimensional units of mass ($M$), length ($L$) and time ($T$). Out of the 11 ($n$) key influencing variables, three ($j$) convenient repeating variables are chosen: the elastic modulus of sand ($E_s$), density of the sand bed ($\rho_s$) and equivalent weight of TNT ($W$). The problem is now reduced to a function of 8 ($k = n–j$) dimensionless variables.

The function $f$ which governs the integrated system is represented as

$$f(\mathrm{Dob}, \mathrm{EI}, E_s, \rho_s, \phi, W, R, t_d, P_5, \delta, \varepsilon) = 0 \quad (3)$$

The dimensionless parameters ($\pi_1$ to $\pi_8$) can be identified in the function $g$

$$g(\pi_1, \pi_2, \pi_3, \pi_4, \pi_5, \pi_6, \pi_7, \pi_8) = 0 \quad (4)$$

$$5.\quad g\left(\text{Dob.}\sqrt[3]{\frac{\rho_s}{W}}, \frac{\text{EI}}{E_s}.\sqrt[3]{\frac{\rho_s^4}{W^4}}, \phi, R.\sqrt[3]{\frac{\rho_s}{W}}, t_d.\frac{\sqrt{E_s}}{\sqrt[3]{W\rho_s^{1/2}}}, P_5, \delta.\sqrt[3]{\frac{\rho_s}{W}}, \varepsilon\right) = 0$$

Let us consider an output dimensionless parameter, say the deflection term ($\pi_7$)

$$6.\quad \pi_7 = h(\pi_1, \pi_2, \pi_3, \pi_4)$$

$$7.\quad \delta\sqrt[3]{\frac{\rho_s}{W}} = h(\pi_1, \pi_2, \pi_3, \pi_4)$$

The ratio of deflection parameter of the prototype to the model (where subscripts m and p mean model and prototype, respectively) yields

$$8.\quad \frac{\delta_p/\left(\sqrt[3]{W/\rho_s}\right)_p}{\delta_m/\left(\sqrt[3]{W/\rho_s}\right)_m} = \frac{h\left((\pi_1)_p, (\pi_2)_p, (\pi_3)_p, (\pi_4)_p\right)}{h\left((\pi_1)_m, (\pi_2)_m, (\pi_3)_m, (\pi_4)_m\right)}$$

The prototype and the model are physically the same, if all the four $\pi$-parameters shown in Equation 7 are the same for the prototype and the model (when scaled). This ensures that the right-hand side of Equation 8 is unity. Moreover, it is important to maintain the material properties ($E_s$ and $\rho_s$) for the sand deposit in the model to be same as that of an actual condition (prototype).

Rearranging Equation 8

$$9.\quad \delta_p = \frac{\left(\sqrt[3]{W/\rho_s}\right)_p}{\left(\sqrt[3]{W/\rho_s}\right)_m}\delta_m = \frac{\sqrt[3]{(W)_p}}{\sqrt[3]{(W)_m}}\delta_m, \quad \text{when } (E_s)_p = (E_s)_m \text{ and } (\rho_s)_p = (\rho_s)_m$$

Finally, scaling coefficient $\lambda$ is deduced

$$10.\quad \delta_m = \lambda\delta_m, \quad \text{where } \lambda = \sqrt[3]{\frac{(W)_p}{(W)_m}}$$

A similar procedure is carried out for the rest of the variables and the appropriate scaling factors are derived (listed in Table 1).

It is assumed that the surface blast wave phenomenon being investigated can be addressed using the aluminium pipe model with a definitive set of variables. Normally, the diameter of the pipes (ID) for oil pipelines varies from 50 to 300 mm depending on the system and requirements, and the depth of the overburden cover ranges from 500 mm to several metres (Kennedy, 1993). For example, let us consider a prototype test condition (case 2) with a scale coefficient $\lambda = 2$, the input parameters of the model are completely scaled using the scaling factor. As emphasised before, the material properties of the sand bed are maintained identical in the model (test case 1) and the prototype (case 2) (necessary conditions). The pipe dimensions are obtained by adopting the scaling law for the stiffness parameter by incorporating the elastic modulus relation between the cast iron prototype pipe and the aluminium model pipe ($E_{p(\text{cast iron})} = 2E_{m(\text{Al})}$, sufficient condition)

$$11.\quad (\text{EI})_p = \lambda^4(\text{EI})_m$$

$$12.\quad E_{\text{C.iron}}\frac{\pi}{64}\left\{(\text{ID}+T)^4_{\text{C.iron}} - (\text{ID})^4_{\text{C.iron}}\right\} = \lambda^4.E_{\text{Al}}\frac{\pi}{64}\left\{(\text{ID}+T)^4_{\text{Al}} - (\text{ID})^4_{\text{Al}}\right\}$$

In the same manner, peak pressure and positive phase duration values are obtained by multiplying the scaled factor of 1 and $\lambda$, respectively. The results confirm the validity of Hopkinson–Cranz scaling law (also known as cube-root scaling law). The observer at a distance $R$ from the centre of an explosive source will be subjected to a blast wave with a pressure amplitude of $P$, positive duration $t_d$ and impulse $I$. The Hopkinson–Cranz scaling law then states for an observer stationed at a distance $\lambda R$ from the centre of a similar explosive will feel a blast wave of amplitude $P$, positive duration $\lambda t_d$ and impulse $\lambda I$. The law implies that for the same value of $Z$, quantities with the dimension of pressure and weighted positive phase ($t_d/W^{1/3}$) remain unchanged through scaling (Baker *et al.*, 1973). Similar results are obtained in this study (see the output variables in Table 1), the $P_5$ value remains identical in cases 1 and 2 and the $t_d$ value is scaled by a factor ($\lambda$) which is a ratio of the cube root of TNT weights of prototype to the model.

Moreover, the determination of coefficient $\lambda$ is not straightforward, which not only depends on the desired prototype diameter and stiffness ratio but also on the explosion event (weight of the TNT explosive). For a an explosion of specific charge at a stand-off distance, the scaled blast wave is to be recreated in the laboratory with the appropriate shock tube configuration. It however involves many trial cases with different rupture pressures and varying dimensions to match the air-blast

parameters. The shock tube used in this study can be applicable to a blast condition with $z$ values ranging from 1·49 to 2·29, with peak pressures ranging from 0·4 to 1·6 MPa. By using scaling laws, with one's own discretion in interpreting the actual blast event, the shock tube-based study can be effectively used for a wide range of blast conditions.

Let us consider a test case 2 with $\lambda = 2$, the scaled test condition involves a TNT explosion of 160 kg at an altitude of 10 m above the ground surface. The summary of the scaled values for test case 2 is listed in Table 1. A blast wave with a peak reflected pressure amplitude of 0·8 MPa and a positive time duration of 6·68 ms strikes the ground surface, embedded with a cast iron pipe ($ID_{C.iron} = 47{\cdot}5$ mm, $OD_{C.iron} = 50$ mm) at a depth of 150 mm. The permanent (plastic) crown deflection for the cast iron pipe in test case 2 is predicted to be 2·3 mm.

## 5. Numerical simulation and discussion

The response of the buried pipe under air-blast impact is examined in more detail by performing numerical simulations. Consequently, the results are then used to validate the predicted values obtained from the dimensional analysis through small-scale shock tube experiments. Numerical models with two different pipe diameters, located at two different burial depths in a sand deposit having identical material properties, are simulated for two specific spherical air-blast test conditions. The two test cases are chosen such that case 1 parameters match exactly with the shock tube experiment configuration, while case 2 values are obtained from the dimensional analysis results for a scaling factor ($\lambda$) of 2. The input variable of Table 1 presents the test conditions for cases 1 and 2, which includes geometric and material values, weight of TNT explosive and the altitude of explosion from the sand surface.

A three-dimensional finite-element model is developed using the commercial code Abaqus/Explicit 6.12 (Abaqus, 2009). A three-noded linear triangular shell element (Abaqus S3R) has been used together with eight-noded hexahedral linear brick elements (Abaqus C3D8R) for modelling the pipe and the surrounding sand medium, respectively. The elastic–perfectly plastic Mohr–Coulomb material model considered for the sand and the pipe is modelled using an elastic–plastic material constitutive law. The sand properties are assumed to be similar in test cases 1 and 2; the Mohr–Coulomb parameters are obtained from Hegde and Sitharam (2015) (same sand samples are used in the present experimental study). The material properties of sand sample used are as follows: Young's modulus, $E = 15$ MPa; Poisson's ratio, $\upsilon = 0{\cdot}3$; cohesion, $c = 0$ kPa; friction and dilation angles are 35° and 24°, respectively. The elastic properties of aluminium pipe are determined from the tensile test ($E_{al} = 68{\cdot}9$ MPa; $\upsilon = 0{\cdot}33$); the yield stress corresponding to 0·2% strain is found to be 40 MPa. From Table 1, the stiffness of the pipe for case 2 is 29 818·3 N m$^2$; this value corresponds to a pipe made of cast iron ($E_{ci} = 140$ MPa) with dimension (OD = 50 mm; ID of 47·5 mm). The elastic–plastic material property of cast iron is obtained from Liu (2009).

The blast loading simulations in Abaqus are based on an empirical method developed by Kingery and Bulmash (1984), where the air-blast parameters from spherical air bursts are predicted by equations. These equations are implemented in Abaqus as a blast function code, ConWep (conventional weapons effects). Researchers have found very good correlation between the use of ConWep and the field experiments with explosives (Henchie *et al.*, 2014; Hyde, 1988; Spranghers *et al.*, 2013). Further, it should be noted that the higher order polynomial coefficient (Shin *et al.*, 2014) used to quantify shock tube blast parameters in Section 3.1 is also obtained by matching the empirical data of Kingery and Bulmash (1984). ConWep function has inputs of spherical air burst of TNT equivalent mass (case 1 = 20 kg, case 2 = 160 kg) and stand-off distance between the ground surface and the source of detonation (case 1 = 5 m, case 2 = 10 m).

Inspection of Figure 7, displacement–time response of the crown of the pipes, shows that the pipe has gone through a plastic deformation after experiencing a peak deflection. The numerical results for the displacement of the pipe for cases 1 and 2 are shown in Figure 8; the contours shown are the residual (plastic) deflection experienced by the pipe at the end of the blast duration. The maximum axial strain is equal to

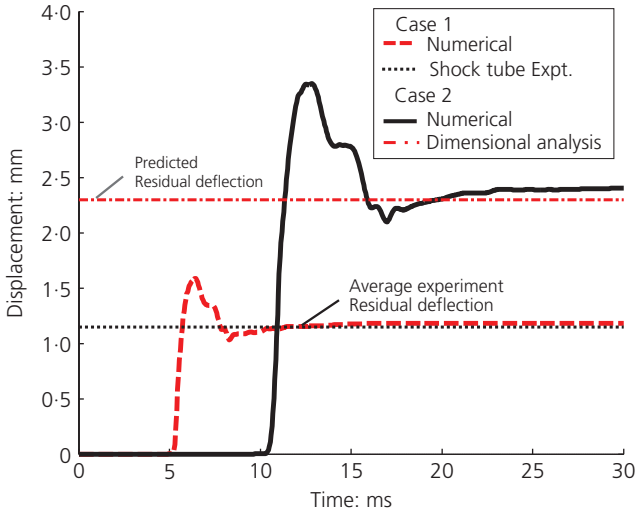


**Figure 7.** Crown displacement responses at centre of the pipe for cases 1 and 2

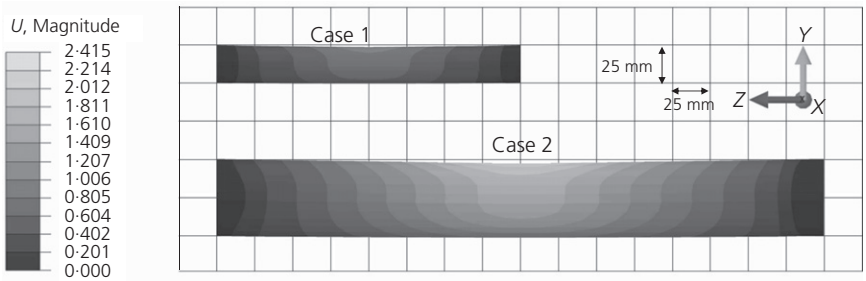


**Figure 8.** Displacement contours of aluminium and cast-iron pipe of test cases 1 and 2

751 με (at $L/3$ on the crown) for case 1. The comparison with the experimental value demonstrates the adequacy of numerical simulation (Figure 6). The maximum crown deflections of the pipe for cases 1 and 2 are 1·58 and 3·34 mm, respectively, whereas the permanent deflections of the pipe (at $L/2$ on the crown) for case 1 are observed to be 1·18 and 2·41 mm for case 2. The simulated residual displacement remarkably matches very well with both the experimental and dimensional analysis values (dashed line in Figure 7).

It is therefore evident from the numerical simulations that the shock tube-based technique can be considered as a reliable and safe alternative method for testing the buried structures exposed to air-blast loads. The shock tube used in this study can generate a blast wave for a scaled distance ($Z$) value between 1·49 and 2·29 and is successful in generating blast waves of medium intensity with peak overpressure <2 MPa. However, the limitation of this study is that the shock tube does not recreate the thermal radiation involved during explosion and hence fail to consider the effects such as fragmentation and/or fusing of sand particles. Further, it is to be noted that the other blast effect such as crater formation and its effect on the buried structure are not included in this study, which plays an important role in large explosions. Hence, the shock tube-based scaling method presented in this study is effective in predicting the response of buried pipelines in low-to-medium air-blast conditions.

## 6. Summary and conclusion

This work uses the dimensional analysis framework in developing an integrated system for studying the effect of spherical air bursts on buried pipelines. A shock tube is used to generate a blast wave which is represented as a scaled estimate of a real blast phenomenon. With necessary and sufficient conditions, non-dimensional input and output parameters are expressed as a function of the equivalent TNT weights.

The results from the experimental study have demonstrated the capability of the shock tube in delivering blast waves without the use of explosives. The shock tube technique is safe, reproducible and more importantly provides versatility of generating blast waves of varying peak pressures and impulse. Further, results from the experiment confirm that blast wave energy has been dissipated in the sand in the form of compression stress waves. The stress attenuation in sand is observed to be less predominant at shallow depths and is found to increase with depth. It is observed that after the blast wave impact, the embedded pipe specimen undergoes residual deflection. The phenomenological details of air-blast loading on the buried pipe are captured using finite-element simulations.

A numerical model of the shock tube experiment is developed and validated against the available experimental results. The permanent deflections obtained from the shock tube experiment match very well with the numerical ConWep simulations of the air-blast loading. Further, numerical results for the scaled model are in good agreement with the predicted values obtained from dimensional analysis. Reduced-scale, shock tube-based experimental technique is found to be a reliable testing option for investigating the interactions of blast wave with the buried structures. The experimentally generated stress and strain values in the pipe will contribute significantly to the design of buried pipelines. In addition, the results from the experiments can be used to validate various numerical and analytical models.

## Acknowledgements

The experiments were performed at the Laboratory for Hypersonic and Shock Wave Research (LHSR) at the Department of Aerospace Engineering, Indian Institute of Science, Bangalore. The authors acknowledge the efforts of their colleagues and the non-technical staffs in LHSR and Soil Mechanics Laboratory, at the Indian Institute of Science. The work was supported by grants provided by DST, Government of India and International Bilateral Cooperation Division, Indo-German (DST-BMBF) cooperation in civil security research (F. No. IBC/FR6/BMBF/CSR/R-03/2015).

**REFERENCES**

Abaqus (2009) *Abacus/Explicit Users' Manual*. Simulia Corp, Providence, RI, USA.

Aune V, Fagerholt E, Langseth M and Borvik T (2016) A shock tube facility to generate blast loading on structures. *International Journal of Protective Structures* **7(3)**: 340–366.

Baker WE, Westine PS and Dodge FT (1973) *Similarity Methods in Engineering Dynamics: Theory and Practice of Scale Modeling*. Hayden Books, Rochelle Park, NJ, USA.

Britan A, Jiang JP, Igra O, Elperin T and Ben-Dor G (1997) Gas filtration during the impact on weak shock waves on granular layers. *International Journal of Multiphase Flow* **23(3)**: 473–491.

Chandra N, Ganpule S, Kleinschmit N *et al.* (2012) Evolution of blast wave profiles in simulated air blasts: experiment and computational modeling. *Shock Waves* **22(5)**: 403–415.

Colombo M, Di Prisco M and Martinelli P (2011) A new shock tube facility for tunnel safety. *Experimental Mechanics* **51(7)**: 1143–1154.

Colombo M, Di Prisco M and Martinelli P (2013) Layered high performance concrete plates interacting with granular soil under blast loads: an experimental investigation. *European Journal of Environmental and Civil Engineering* **17(10)**: 1002–1025.

De A and Zimmie TF (2007) Centrifuge modeling of surface blast effects on underground structures. *Geotechnical Testing Journal ASTM* **30(5)**: 427–431.

De A, Morgante AN and Zimmie TF (2016) Numerical and physical modeling of geofoam barriers as protection against effects of surface blast on underground tunnels. *Geotextile and Geomembrane* **44(1)**: 1–12.

Hegde A and Sitharam TG (2015) Experimental and numerical studies on protection of buried pipelines and underground utilities using geocells. *Geotextiles and Geomembranes* **43(5)**: 372–381.

Henchie TF, Chung KYS, Nurick GN, Ranwaha N and Balden VH (2014) The response of circular plates to repeated uniform blast loads: an experimental and numerical study. *International Journal of Impact Engineering* **74**: 36–45, https://doi.org/10.1016/j.ijimpeng.2014.02.021.

Hyde DW (1988) *User's Guide for Microcomputer Programs ConWep and FunPro, Applications of TM 5-855-1. Fundamentals of Protective Design for Conventional Weapons*. US Army Engineer Waterways Experiment Station, Springfield, VA, USA.

Kennedy JL (1993) *Oil and Gas Pipeline Fundamentals*, 2nd edn. Pennwell Books, Tulsa, OK, USA.

Kingery CN and Bulmash G (1984) *Air Blast Parameters from TNT Spherical Air Burst and Hemispherical Surface Burst*. Defence Technical Information Center, Ballistic Research Laboratory, Aberdeen, MD, USA, Report BRL, 02555.

Kleinschmit NN (2011) *A Shock Tube Technique for Blast Wave Simulation and Studies of Flow Structure Interactions in Shock Tube Blast Experiments*. MS thesis, University of Nebraska-Lincoln, Lincoln, NE, USA.

Koneshwaran S, Thambiratnam PD and Gallage C (2015) Response of segmented bored transit tunnels to surface blast. *Advances in Engineering Software* **89**: 77–89, https://doi.org/10.1016/j.advengsoft.2015.02.007.

Liu H (2009) Dynamic analysis of subway structures under blast loading. *Geotechnical and Geological Engineering* **27(6)**: 699–711.

Newman AJ and Mollendorf JC (2010) The peak overpressure field resulting from shocks emerging from circular shock tubes. *Journal of Fluids Engineering* **132(8)**: 81204.

Olarewaju AJ, Kameswara Rao NSV and Mannan MA (2010) Response of underground pipes due to blast loads by simulation – an overview. *Electronic Journal of Geotechnical Engineering* **15/G**: 831–852.

Shin J, Whittaker A and Amjad A (2014) *Air-Blast Effects on Civil Structures*. Multidisciplinary Center for Earthquake Engineering Research, State University of New York, Buffalo, NY, USA, Report MCEER-14-0006.

Spranghers K, Vasilakos I, Lecompte D, Sol H and Vantomme J (2013) Numerical simulation and experimental validation of the dynamic response of aluminum plates under free air explosions. *International Journal of Impact Engineering* **54**: 83–95, https://doi.org/10.1016/j.ijimpeng.2012.10.014.

USDoD (US Department of Defence) (2008) *UFC 3-340-02: Structures to Resist the Effects of Accidental Explosions*. US Department of Defence, Washington, DC, USA.

Vivek P and Sitharam TG (2017) Sand ejecta kinematics and impulse transfer associated with the buried blast loading: a controlled laboratory investigation. *International Journal of Impact Engineering* **104**: 85–94, https://doi.org/10.1016/j.ijimpeng.2017.02.017.

Xu GF, Deng ZD, Deng FF and Liu GB (2013) Numerical simulation on the dynamic response of buried pipelines subjected to blast loads. *Advanced Materials Research* **671–674**: 519–522, http://dx.doi.org/10.4028/www.scientific.net/AMR.671-674.519.

Zhang L, Liang Z and Zhang J (2016) Mechanical response of a buried pipeline to explosion loading. *Journal of Failure Analysis and Prevention* **16(4)**: 576–582.

Zhao X, Tiwari V, Sutton MA *et al.* (2013) Scaling of the deformation histories for clamped circular plates subjected to blast loading by buried charges. *International Journal of Impact Engineering* **54**: 31–50, https://doi.org/10.1016/j.ijimpeng.2012.10.016.